A generalized non-reflecting inlet boundary condition for steady and forced compressible flows with injection of vortical and acoustic waves

Guillaume Daviller, Gorkem Oztarlik, Thierry Poinsot

▶ **To cite this version:**

Guillaume Daviller, Gorkem Oztarlik, Thierry Poinsot. A generalized non-reflecting inlet boundary condition for steady and forced compressible flows with injection of vortical and acoustic waves. Computers and Fluids, 2019, 190, pp.503-513. 10.1016/j.compfluid.2019.06.027 . hal-02538669

HAL Id: hal-02538669
https://hal.science/hal-02538669

Submitted on 9 Apr 2020

HAL is a multi-disciplinary open access archive for the deposit and dissemination of scientific research documents, whether they are published or not. The documents may come from teaching and research institutions in France or abroad, or from public or private research centers.

L'archive ouverte pluridisciplinaire **HAL**, est destinée au dépôt et à la diffusion de documents scientifiques de niveau recherche, publiés ou non, émanant des établissements d'enseignement et de recherche français ou étrangers, des laboratoires publics ou privés.

OATAO

Open Archive Toulouse Archive Ouverte

OATAO is an open access repository that collects the work of Toulouse researchers and makes it freely available over the web where possible

This is an author's version published in: http://oatao.univ-toulouse.fr/25689

Official URL:

https://doi.org/10.1016/j.compfluid.2019.06.027

To cite this version:

Daviller, Guillaume and Oztarlik, Gorkem and Poinsot, Thierry *A generalized non-reflecting inlet boundary condition for steady and forced compressible flows with injection of vortical and acoustic waves.* (2019) Computers and Fluids, 190. 503-513. ISSN 0045-7930 .

Any correspondence concerning this service should be sent to the repository administrator: tech-oatao@listes-diff.inp-toulouse.fr

A generalized non-reflecting inlet boundary condition for steady and forced compressible flows with injection of vortical and acoustic waves

G. Daviller[a,*], G. Oztarlik[b], T. Poinsot[b]

[a] CERFACS, Toulouse 31100, France
[b] IMF Toulouse, INP de Toulouse and CNRS, France

Characteristic boundary conditions
Non reflecting boundary conditions
Turbulence injection
Acoustic forcing

This paper describes a new boundary condition for subsonic inlets in compressible flow solvers. The method uses characteristic analysis based on wave decomposition and the paper discusses how to specify the amplitude of incoming waves to inject simultaneously three-dimensional turbulence and one-dimensional acoustic waves while still being non-reflecting for outgoing acoustic waves. The non-reflecting property is ensured by using developments proposed by Polifke et al. [1, 2]. They are combined with a novel formulation to inject turbulence and acoustic waves simultaneously at an inlet. The paper discusses the compromise which must be sought by the boundary condition formulation between conflicting objectives: respecting target unsteady inlet velocities (for turbulence and acoustics), avoiding a drift of the mean inlet velocities and ensuring non-reflecting performances for waves reaching the inlet from the computational domain. This well-known limit of classical formulations is improved by the new approach which ensures that the mean inlet velocities do not drift, that the unsteady components of velocity (turbulence and acoustics) are correctly introduced into the domain and that the inlet remains non-reflecting. These properties are crucial for forced unsteady flows but the same formulation is also useful for unforced cases where it allows to reach convergence faster. The method is presented by focusing on the expression of the ingoing waves and comparing it with the classical NSCBC approach [3]. Four tests are then described: (1) the injection of acoustic waves through a non reflecting inlet, (2) the compressible flow establishment in a nozzle, (3) the simultaneous injection of turbulence and ingoing acoustic waves into a duct terminated by a reflecting outlet and (4) a turbulent, acoustically forced Bunsen-type premixed flame.

1. Introduction

Specifying boundary conditions for compressible flow simulations is still a major issue in many fields such as astrophysics [4,5], aerodynamics and aeroacoustics [6–11] or combustion instabilities and noise [2,12–16]. The present paper focuses on a limited part of this problem: the specification of inlet boundary conditions in subsonic compressible flows. Its objective is to construct a boundary condition which should satisfy three properties:

- P1 - Provide a well-posed formulation for the Navier–Stokes equations as well as perfectly non-reflecting inlet properties
- P2 - Allow to inject plane acoustic waves
- P3 - Allow to inject three-dimensional turbulence

* Corresponding author.
E-mail address: daviller@cerfacs.fr (G. Daviller).

It is important to satisfy P1, P2 and P3 simultaneously: the capability to inject ingoing acoustic waves and turbulence at the same time on an inlet patch while letting outgoing acoustic waves cross the boundary without reflection is crucial in many configurations. Well-known examples include the determination of the transfer function of turbulent flames [15,17], the prediction of combustion noise in gas turbines [18–20] or the evaluation of the acoustic transfer matrix of singular elements in turbulent flows [21–24]. All these studies require to introduce harmonic acoustic forcing and turbulence on the same inlet boundary while letting acoustic waves propagate from the computational domain to the outside without reflection (Fig. 1). Similarly, studies of combustion noise in gas turbines [20,25,26] require to perform simulations of the noise produced by a jet forced simultaneously by turbulence and by acoustic waves generated in the combustion chamber.

This paper uses characteristic boundary conditions [3,4,27] which have become the standard approach in most

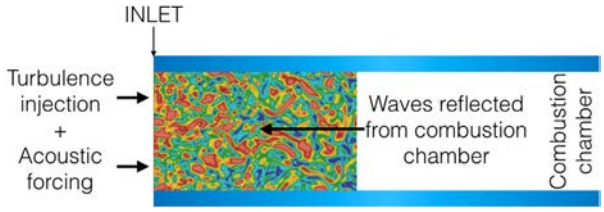

Fig. 1. An example where turbulence and acoustic waves must be introduced through the inlet of a compressible simulation while acoustic waves reflected from the computational domain must propagate without reflection through the same surface: the computation of the Flame Transfer Function of a turbulent flame [15].

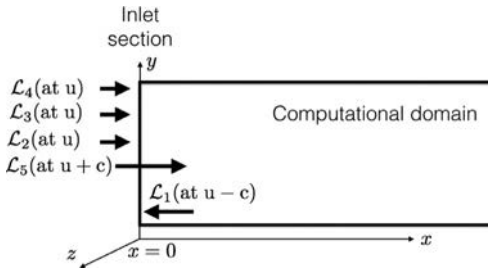

Fig. 2. Characteristic waves at a subsonic inlet (inlet at $x = 0$).

compressible solvers [11,28–30]. These methods use characteristic analysis to decompose the Navier–Stokes equations at the boundary[1] and identify waves going into the domain and waves leaving the domain. Wave amplitudes can be expressed as spatial derivatives of the primitive variables. The amplitudes of waves leaving the domain depend only on the flow within the computational domain: they can be computed using one-sided derivatives of the resolved field inside this domain. Inversely, the amplitudes of the waves entering the computational domain can not be obtained by differentiating the field in the domain because this would lead to an ill-posed problem: they must be imposed using information given by the boundary conditions. Fig. 2 shows that, for a subsonic inlet, only the outgoing acoustic wave $\mathcal{L}_1$ (see Section 2 for wave definitions) is leaving the computational domain at speed $u - c$ where u is the local convection velocity and c the local sound speed. All other waves (the acoustic wave $\mathcal{L}_5$ at speed $u + c$, the entropy wave $\mathcal{L}_2$ at speed u and the two transverse waves $\mathcal{L}_3$ and $\mathcal{L}_4$ at speed u) are entering the domain and must be specified using the boundary conditions. This paper focuses on the determination of these incoming wave amplitudes.

Section 2 recalls the basis of the NSCBC (Navier Stokes Characteristic Boundary Conditions) technique applied to an inlet. The specification of the incoming waves is presented in Section 3 and a novel inlet condition able to satisfy properties P1–P3 is discussed (called NRI-NSCBC for Non Reflecting Inlet NSCBC). Before performing any simulation, a simple theoretical approach is used to predict the reflection coefficient of the standard NSCBC formulation and of the new NRI-NSCBC condition for the injection of acoustic waves in one dimension (Section 4). These results are validated using a one-dimensional simulation of a forced duct in Section 5. The impact of the NRI-NSCBC formulation is then illustrated through three examples[2]:

- Section 6 shows that, for an unforced multi-dimensional flow (a nozzle case), using the NRI-NSCBC condition allows to eliminate acoustic waves and to converge much faster to steady state, a crucial property for compressible flow solvers which often remain limited by small time steps and long computation times before convergence.
- Section 7 presents an example of simultaneous acoustic forcing and turbulence injection in a three-dimensional channel and shows that the NRI-NSCBC is able to satisfy Properties 1–3 simultaneously.
- Finally Section 8 proposes a DNS of a premixed turbulent flame which is forced acoustically using both boundary conditions formulations.

2. Characteristic inlet boundary condition for subsonic flows

Consider a subsonic inlet (Fig. 2) where the boundary plane is the (y, z) plane. The velocity components to impose at this inlet are (u^t, v^t, w^t). These components can be steady or change with time when turbulence and/or acoustic waves are injected through the inlet. Note that these fields are "target" values: they correspond to the injected velocity signals which must be imposed at the inlet, not necessarily to the values (u, v, w) which will be actually reached during the computation because outgoing reflected waves (coming from the computational domain) also change the velocity and pressure field on the inlet patch (Fig. 1).

The Navier–Stokes equations at the inlet can be recast in terms of waves propagating in the x direction, leaving the other two directions unchanged:

$$\frac{\partial \rho}{\partial t} + d_1 + \frac{\partial}{\partial y}(\rho v) + \frac{\partial}{\partial z}(\rho w) = 0 \tag{1}$$

$$\frac{\partial(\rho E)}{\partial t} + \frac{1}{2}\left(u^2 + v^2 + w^2\right)d_1 + \frac{d_2}{\gamma - 1} + \rho u d_3 + \rho v d_4 + \rho w d_5 + \frac{\partial}{\partial y}[v(\rho e_s + p)] + \frac{\partial}{\partial z}[w(\rho e_s + p)] = \nabla(\lambda \nabla T) + \nabla(u.\tau) \tag{2}$$

$$\frac{\partial(\rho u)}{\partial t} + u d_1 + \rho d_3 + \frac{\partial}{\partial y}(\rho v u) + \frac{\partial}{\partial z}(\rho w u) = \frac{\partial \tau_{1j}}{\partial x_j} \tag{3}$$

$$\frac{\partial(\rho v)}{\partial t} + v d_1 + \rho d_4 + \frac{\partial}{\partial y}(\rho v v) + \frac{\partial}{\partial z}(\rho w v) + \frac{\partial p}{\partial y} = \frac{\partial \tau_{2j}}{\partial x_j} \tag{4}$$

$$\frac{\partial(\rho w)}{\partial t} + w d_1 + \rho d_5 + \frac{\partial}{\partial y}(\rho v w) + \frac{\partial}{\partial z}(\rho w w) + \frac{\partial p}{\partial z} = \frac{\partial \tau_{3j}}{\partial x_j} \tag{5}$$

where τ is the viscous stress tensor. e_s and E are the sensible and total energies respectively:

$$e_s = \int_{To}^{T} C_v dT \quad \text{and} \quad E = e_s + \frac{1}{2}(u^2 + v^2 + w^2) \tag{6}$$

The system of Eqs. (1) to (5) contains derivatives normal to the x boundary (d_1 to d_5), derivatives parallel to the x boundary (called "transverse terms"), and viscous terms. The vector **d** is given by characteristic analysis:

[1] Note that more sophisticated methods such as Perfectly Matched Layers [31–33] can be used to make boundaries fully non-reflecting for multidimensional flows in other fields such as electromagnetism or aeroacoustics. These methods are used mainly in infinite domains while characteristic-based methods are usually preferred in inlet/outlet/ configurations.

[2] Note that the present paper focuses on inlet boundary conditions: readers are referred to [2,34,35] which discuss similar methods for outlets.

$$\mathbf{d} = \begin{pmatrix} d_1 \\ d_2 \\ d_3 \\ d_4 \\ d_5 \end{pmatrix} = \begin{pmatrix} \frac{1}{c^2}\left[\mathcal{L}_2 + \frac{1}{2}(\mathcal{L}_5 + \mathcal{L}_1)\right] \\ \frac{1}{2}(\mathcal{L}_5 + \mathcal{L}_1) \\ \frac{1}{2\rho c}(\mathcal{L}_5 - \mathcal{L}_1) \\ \mathcal{L}_3 \\ \mathcal{L}_4 \end{pmatrix} = \begin{pmatrix} \frac{\partial(\rho u)}{\partial x} \\ \rho c^2 \frac{\partial u}{\partial x} + u\frac{\partial p}{\partial x} \\ u\frac{\partial u}{\partial x} + \frac{1}{\rho}\frac{\partial p}{\partial x} \\ u\frac{\partial v}{\partial x} \\ u\frac{\partial w}{\partial x} \end{pmatrix} \tag{7}$$

where c is the local speed of sound given by $c^2 = \gamma p/\rho$ and the $\mathcal{L}_i$'s are the amplitudes of characteristic waves propagating at the characteristic velocities $u - c$, u and $u + c$:

$$\mathcal{L}_1 = (u - c)\left(\frac{\partial p}{\partial x} - \rho c \frac{\partial u}{\partial x}\right) \tag{8}$$

$$\mathcal{L}_2 = u\left(c^2 \frac{\partial \rho}{\partial x} - \frac{\partial p}{\partial x}\right) \tag{9}$$

$$\mathcal{L}_3 = u\frac{\partial v}{\partial x} \quad \text{and} \quad \mathcal{L}_4 = u\frac{\partial w}{\partial x} \tag{10}$$

$$\mathcal{L}_5 = (u + c)\left(\frac{\partial p}{\partial x} + \rho c \frac{\partial u}{\partial x}\right) \tag{11}$$

3. Specification of incoming waves

For a subsonic three-dimensional inlet, the problem is well posed if four conditions are imposed [3,36]. In a characteristic based method such as NSCBC, this means that the four incoming waves $\mathcal{L}_2, \mathcal{L}_3, \mathcal{L}_4$ and $\mathcal{L}_5$ must be imposed. The outgoing wave $\mathcal{L}_1$ does not depend on the boundary conditions and can be computed using one-sided derivatives of the field inside the computational domain. Therefore, the solution can be advanced in time on the inlet, using the system of Eqs. (1) to (5) for boundary values if an evaluation for $\mathcal{L}_2$ to $\mathcal{L}_5$ can be found. The principle of NSCBC is to evaluate these wave amplitudes as if the flow was locally one-dimensional and inviscid (LODI). LODI equations provide an estimation of the wave amplitudes $\mathcal{L}_i$ which is usually chosen so that the physical boundary condition is satisfied. Usual LODI equations are:

$$\frac{\partial \rho}{\partial t} + \frac{1}{c^2}\left(-\mathcal{L}_2 + \frac{1}{2}(\mathcal{L}_5 + \mathcal{L}_1)\right) = 0 \tag{12}$$

$$\frac{\partial u}{\partial t} + \frac{1}{2\rho c}(\mathcal{L}_5 - \mathcal{L}_1) = 0 \tag{13}$$

$$\frac{\partial v}{\partial t} + \mathcal{L}_3 = 0 \tag{14}$$

$$\frac{\partial w}{\partial t} + \mathcal{L}_4 = 0 \tag{15}$$

$$\frac{\partial p}{\partial t} + \frac{1}{2}(\mathcal{L}_5 + \mathcal{L}_1) = 0 \tag{16}$$

The difficult question and the differentiating factor between characteristic methods is the specification of the ingoing wave amplitudes $\mathcal{L}_2, \mathcal{L}_3, \mathcal{L}_4$ and $\mathcal{L}_5$ as a function of the chosen inlet conditions. For example, for a constant velocity inlet, the LODI equation (13) would suggest that the incoming acoustic wave amplitude $\mathcal{L}_5$ should be equal to the outgoing wave $\mathcal{L}_1$ but this approach is often too simple for unsteady cases.[3] For the sake of simplicity, the presentation is limited now to an isentropic inlet where the entropy wave $\mathcal{L}_2$ is set to zero. Using Eqs. (13)–(15), the LODI expression for such an isentropic inlet is to write the incoming waves as:

$$\mathcal{L}_5 = -2\rho c \frac{\partial u^t}{\partial t},\ \mathcal{L}_3 = -\frac{\partial v^t}{\partial t} \text{ and } \mathcal{L}_4 = -\frac{\partial w^t}{\partial t} \tag{17}$$

which allows to inject an unsteady signal of components (u^t, v^t, w^t). Unfortunately, Eq. (17) does not work in practice for three reasons:

1. For a steady inlet ($u^t = v^t = w^t =$ constant), this condition is perfectly reflecting as the ingoing waves $\mathcal{L}_3$, $\mathcal{L}_4$ and $\mathcal{L}_5$ are all exactly zero: the solver knows that the inlet velocity is constant but it has no information on the values of the target velocities so that, in multidimensional configurations, the mean inlet velocities usually drift because of transverse and viscous terms present in the system of Eqs. (1) to (5). This is usually corrected by adding a linear relaxation term to the target values u^t, v^t and w^t as proposed initially by Rudy and Strikwerda [36,38]. For the normal velocity u, the ingoing acoustic wave $\mathcal{L}_5$ becomes:
$$\mathcal{L}_5 = \rho c\left(-2\frac{\partial u^t}{\partial t} + 2\ K(u - u^t)\right) \tag{18}$$
while the two transverse waves are written:
$$\mathcal{L}_3 = -\frac{\partial v^t}{\partial t} + 2\ K(v - v^t) \quad \text{and} \quad \mathcal{L}_4 = -\frac{\partial w^t}{\partial t} + 2K(w - w^t) \tag{19}$$
Terms such as $(u - u^t)$ are called "relaxation" terms [36,38]. They do not have a theoretical basis[4]: they offer the simplest linear correction form which can be added to the NSCBC theory to avoid a drift of mean values as it forces the instantaneous velocity u to go to its target value u^t with a relaxation time $1/K$. Independently of its exact form, this term in Eq. (18) is sufficient to avoid drifting mean inlet speed values when K is "sufficiently" large but it also deteriorates the non-reflecting character of the inlet as will be shown later. Transverse waves ($\mathcal{L}_3$ and $\mathcal{L}_4$) raise no difficulty as they are not associated to any axial acoustic wave and will not be discussed any more in the rest of the paper.
2. An interesting issue in the correction term $(u - u^t)$ of Eq. (18) is how to choose the "target" value u^t. A simple choice would be $u^t = \bar{u} + u^t_+$ where $\bar{u}$ is the target mean velocity and u^t_+ is the target unsteady velocity (either acoustic or vortical) imposed on the inlet patch. A better choice was proposed in [1,2] who pointed out that outgoing acoustic waves (inducing velocity fluctuations which will be called u_-) may also reach the inlet when they propagate from the computational domain to the inlet and should be accounted for in u^t. Fortunately, these outgoing waves can be evaluated in the limit of plane, low-frequency waves using the outgoing wave amplitude $\mathcal{L}_1$ which is readily available in all NSCBC methods. Therefore, the proper way to account for u_- is to add it to the target velocity to have $u^t = \bar{u} + u^t_+ + u_-$.
A last issue linked to Eq. (17) is the choice of the relaxation coefficient K (units: s^{-1}). The proper scaling for K is

[3] One aspect of this problem which is not discussed here is the need to also incorporate transverse terms in the ingoing wave expressions [11,30,37]. At an inlet, these terms play a limited role and they will be omitted throughout the present paper.

[4] A temptative explanation for this expression was actually proposed recently by Pirozzoli and Colonius [10], leading to a similar expression.

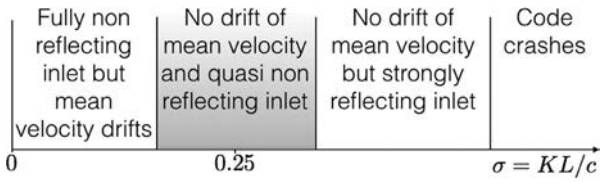

Fig. 3. Typical behavior of the solution for the classical NSCBC inlet condition (Eq. (18)) as a function of the reduced relaxation coefficient $\sigma = KL/c$. L is a typical domain length of the domain and c the sound speed. The shaded area is the desired operational zone.

the reduced factor $\sigma = KL/c$ where L and c are a characteristic length and a typical sound speed of the domain respectively [36,38]. Choosing an adequate value for K is a critical issue in many cases. Very large values of σ can lead to an unstable solution and a divergence of the simulation even in a stable flow (Fig. 3) because the wave amplitude becomes too large as soon as the velocity deviates from its target value: such instabilities are purely numerical and are due to the boundary condition. On the other hand, low values provide non-reflecting characteristics but will let the mean solution to drift from its target mean value $\bar{u}$ because of viscous and transverse terms affecting the solution in the system of Eqs. (1) to (5). Therefore, there usually is a range of σ values which provide both non drifting and quasi non-reflecting properties. Rudy and Strikwerda suggest that this occurs near $\sigma = 0.25$ but in practice, wide ranges of σ have to be tested by NSCBC users, leading to inefficient trial and error procedures. In some cases, large values of K are used, leading to inlets where the velocity is totally fixed but the boundary is fully reflecting.

3. Another and more surprising problem was pointed out by Prosser [39] and confirmed by Guezennec and Poinsot [40]. In the classical NSCBC approach, to inject a perturbation u^t, the incoming wave is expressed as:

$$\mathcal{L}_5 = -2\rho c\frac{\partial u^t}{\partial t} \tag{20}$$

This is a correct formulation to inject acoustic waves but Prosser [39] used a low Mach number expansion of the Navier–Stokes equations to show that the proper expression to inject vortical perturbations was different and that the factor 2 had to be suppressed to have:

$$\mathcal{L}_5 = -\rho c\frac{\partial u^t}{\partial t} \tag{21}$$

The fact that the factor 2 of Eq. (20) used for acoustic wave injection must be removed for vorticity injection in Eq. (21) was confirmed by the analysis of Polifke et al. [1] and tests [40] show that indeed, Eq. (21) is the proper wave expression to inject vortical perturbations (isolated vortices or fully developed turbulence) but raise a simple question: which expression (Eqs. (20) or (21)) should be used in practice? The present paper shows that they actually must be combined as discussed below.

These recent results suggest a generalized formulation for inlet boundary conditions which is the basis for the NRI-NSCBC condition described here[5] In this formulation, ingoing perturbations are split into two separate components which are superposed to the incoming wave amplitude: the vortical fluctuation, corresponding to a signal u_v^t and the acoustic fluctuation corresponding to a signal u_a^t. Each component is handled individually and superposed in the incoming wave as follows:

$$\frac{\mathcal{L}_5}{\rho c} = \underbrace{-2\frac{\partial u_a^t}{\partial t} - \frac{\partial u_v^t}{\partial t}}_{I} + \underbrace{2\,K[u - (\bar{u} + u_a^t + u_v^t + u_-)]}_{II} \tag{22}$$

where part I of expression (22) combines a term $2\partial u_a^t/\partial t$ to introduce acoustic waves and another one $\partial u_v^t/\partial t$ to inject turbulence, each of them with the correct factor (2 for acoustics and 1 for turbulence). Part II of expression (22) is the relaxation term. It is introduced to avoid drift and is not proposed by the characteristic theory. It includes u_a^t and u_v^t but also u_- as suggested by Polifke et al. [1]. This formulation allows to use exact terms for $2\partial u_a^t/\partial t$ and $\partial u_v^t/\partial t$ (satisfying properties P2 and P3 introduced in Section 1) while providing an expression for the relaxation term which should be zero as long as non acoustic terms remain small at the inlet (satisfying property P1). This should allow to use large relaxation factors K avoiding the drift of mean values while still being non reflecting for all normal acoustic waves: the relaxation term in Eq. (22) becomes non zero only when viscous and transverse terms become non negligible on the inlet. For all other cases, the relaxation term (II) is zero and Eq. (22) reduces to the exact NSCBC approach for $\mathcal{L}_5$: $\mathcal{L}_5 = -2\rho c\frac{\partial u_a^t}{\partial t} - \rho c\frac{\partial u_v^t}{\partial t}$.

In the expression of the incoming wave $\mathcal{L}_5$ (Eq. (22)), the acoustic velocity u_- associated to the reflected wave reaching the inlet from the computation domain must be evaluated. In the case of an outlet, Polifke et al. [1,41] used a method called CBF (characteristics based filter) to obtain a plane averaged value for the outgoing wave amplitude. This requires introducing a series of planes near the oulet of the computational domain where the outgoing wave can be evaluated. CBF is precise but can be difficult or impossible to implement in cases where the domain outlet has a complex shape or typically at an inlet as studied in the present work. Here an alternative technique is used where u_- is evaluated locally at each point of the inlet patch from the time integral of the acoustic wave amplitude $\mathcal{L}_1$ which is available in NSCBC:

$$u_- = \frac{1}{2\rho c}\int_0^t \mathcal{L}_1 dt \tag{23}$$

Expression (23) for u_- avoids using the PWM approach [1] and can be used in any code using NSCBC boundary conditions.[6]

The following sections compare the new NRI-NSCBC formulation to the classical NSCBC conditions [3,12]. Table 1 summarizes the wave expressions which will be used for both boundary conditions.

Table 1
Comparison of the classical NSCBC and the NRI-NSCBC conditions. $\bar{u}$ is the mean target velocity, u_a^t is the target acoustic fluctuation, u_v^t is the target vortical fluctuation and u_- is the reflected velocity fluctuation reaching the inlet from the computational domain.

Boundary condition	Transverse Waves $\mathcal{L}_3$ and $\mathcal{L}_4$	Axial Wave $\mathcal{L}_5$
NSCBC	$\mathcal{L}_3 = -\frac{\partial v^t}{\partial t}$ and $\mathcal{L}_4 = -\frac{\partial w^t}{\partial t}$	$\frac{\mathcal{L}_5}{\rho c} = -2\frac{\partial u_a^t}{\partial t} - 2\frac{\partial u_v^t}{\partial t}$ $+2K[u - (\bar{u} + u_a^t + u_v^t)]$
NRI-NSCBC	$\mathcal{L}_3 = -\frac{\partial v^t}{\partial t}$ and $\mathcal{L}_4 = -\frac{\partial w^t}{\partial t}$	$\frac{\mathcal{L}_5}{\rho c} = -2\frac{\partial u_a^t}{\partial t} - \frac{\partial u_v^t}{\partial t}$ $+2\,K[u - (\bar{u} + u_a^t + u_v^t + u_-)]$

[5] The reviewing phase of the present paper showed that this result could have been obtained also by combining results proposed by the group of Pr Polifke [1] with the work of Pr Prosser [39].

[6] In practice, for certain cases, Eq. (23) must be high-pass filtered to remove any continuous component.

4. Theoretical analysis of reflection coefficients in one dimension

A first method to analyze the differences between the standard NSCBC and the NRI-NSCBC conditions is to consider a simple case (Fig. 4) such as the inlet of a configuration where waves can be assumed to be one-dimensional. No vortical perturbation is introduced: $u_v^t = 0$. The inlet patch has a constant mean velocity $\bar{u}$ and is submitted to an acoustic harmonic forcing at pulsation ω with a target amplitude u_a^t. A reflected wave inducing an acoustic perturbation u_- associated to a wave amplitude $\mathcal{L}_1$ also reaches the inlet so that the exact velocity fluctuation at the inlet should be $u_a^t + u_-$. At this point u_- could be any signal: the only assumption is that u_- is a reflection due to the acoustic forcing and that it is therefore a harmonic signal at pulsation ω too.

This case allows to derive analytically, what the inlet velocity will be in a code using the boundary conditions of Table 1. To obtain this result, the two ingoing wave formulations of Table 1 are gathered in a single notation for this case with acoustic forcing only and no turbulence injection ($u_v^t = 0$):

$$\frac{\mathcal{L}_5}{\rho c} = -2\frac{\partial u_a^t}{\partial t} + 2\,K[u - (\bar{u} + u_a^t + \alpha u_-)] \tag{24}$$

When $\alpha = 0$, the standard NSCBC condition is obtained while $\alpha = 1$ yields the NRI-NSCBC condition. The reflected wave (amplitude $\mathcal{L}_1$) creates an acoustic velocity u_- which reaches the inlet and interacts with the inlet boundary condition. In general, u_- is never zero: reflected waves are found at the inlet of most compressible computations.

Assuming that all quantities fluctuate at pulsation ω and expressing all variables as $f(t) = Re[\hat{f}\exp(-i\omega t)]$, it is possible to combine Eqs. (24) and (13) to obtain the velocity fluctuations $u' = u - \bar{u}$ at the inlet. To do this, $\mathcal{L}_1$ is obtained from u_- using:

$$\frac{\partial u_-}{\partial t} = \frac{1}{2\rho c}\mathcal{L}_1 \quad \text{so that} \quad \hat{\mathcal{L}}_1 = -2i\omega\rho c\hat{u}_- \tag{25}$$

Eq. (13) can then be used to obtain the inlet velocity fluctuations $\hat{u}'$ using Eq. (24) for $\mathcal{L}_5$ and Eq. (25) for $\mathcal{L}_1$:

$$\frac{\partial u}{\partial t} = -\frac{1}{2\rho c}(\mathcal{L}_5 - \mathcal{L}_1) \tag{26}$$

which leads to:

$$\hat{u}' = \hat{u}_a^t + \frac{K\alpha - i\omega}{K - i\omega}\hat{u}_- \tag{27}$$

Eq. (27) conveys two messages:

- In general, the inlet velocity fluctuation $\hat{u}'$ is not equal to the acoustic forcing amplitude imposed on the boundary $\hat{u}_a^t$. For both boundary conditions ($\alpha = 0$ or 1), the only cases where $\hat{u}'$ is equal to $\hat{u}_a^t$ corresponds to situations where no outgoing wave reaches the inlet ($\hat{u}_- = 0$).
- The exact solution is that the inlet velocity should be the sum of the acoustic contributions coming from left and right: $\hat{u}' = \hat{u}_a^t + \hat{u}_-$. When $\alpha = 1$ (NRI-NSCBC condition), Eq. (27) shows that this property is always satisfied. For the standard NSCBC condition ($\alpha = 0$), the conclusion is opposite: the inlet velocity $\hat{u}'$ is never equal to its theoretical value except in rare cases where $K = 0$ or $\hat{u}_- = 0$.

Knowing $\hat{u}'$, it is also possible to express the inlet wave $\mathcal{L}_5$:

$$\hat{\mathcal{L}}_5 = \hat{\mathcal{L}}_5^t + R_1\hat{\mathcal{L}}_1 \quad \text{with} \quad R_1 = \frac{K(1-\alpha)}{K - i\omega} \tag{28}$$

where $\hat{\mathcal{L}}_5^t = 2i\omega\rho c\hat{u}_a^t$ is the target forcing wave and R_1 can be viewed as the reflection coefficient of the boundary condition: it measures how much of a left going wave $\mathcal{L}_1$ reflects into the ingoing acoustic wave $\mathcal{L}_5$. When $\alpha = 1$ (NRI-NSCBC), R_1 is exactly zero: the inlet is truly non reflecting and the injected wave $\hat{\mathcal{L}}_5$ contains only the imposed wave $\hat{\mathcal{L}}_5^t$. For the standard NSCBC condition ($\alpha = 0$), R_1 is never zero: the inlet is reflecting and any outgoing wave reaching it will be reflected back into the domain, making the inlet effectively more and more reflecting as K is increased. Note that, in this case, the reflection coefficient R_1 in Eq. (28) matches the expression obtained for the reflection coefficient by Selle et al. [34], Polifke et al. [1] and Pirozzoli and Colonius [10].

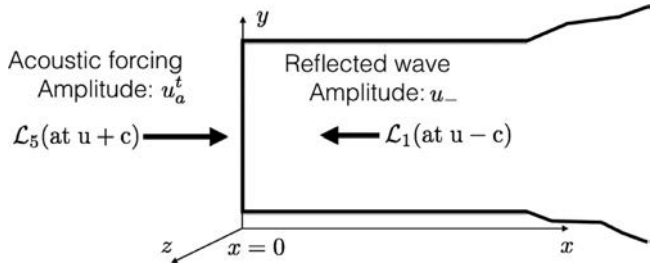

Fig. 4. Characteristic waves at a subsonic inlet (inlet at $x = 0$). The acoustic forcing induces a velocity fluctuation u_a^t. A longitudinal acoustic wave (amplitude u_-) is reaching the inlet from the computation domain.

5. A one-dimensional duct with inlet acoustic forcing

The two boundary conditions of Table 1 are tested first on a one-dimensional duct of length L (Fig. 5) forced acoustically at its inlet ($x = 0$) and terminated by a fixed pressure outlet ($p' = 0$ at $x = L$). This is a direct application of the results of Section 4 where u_- will be specified: the inlet forcing is harmonic and corresponds to a velocity fluctuation $\hat{u}_a^t$. The outlet is fully reflecting so that ingoing waves will reflect at $x = L$ into outgoing waves (u_-) and interact with the inlet condition at $x = 0$. For all test cases presented in this section and the following ones, the compressible Navier–Stokes equations are solved using the fourth-order TTGC scheme (on regular meshes [42]) in the AVBP solver [43,44]. Time advancement is fully explicit and a CFL number of 0.7 is used for all runs.

Since the outlet reflection coefficient is -1 (to ensure $p' = 0$), the ratio between $\mathcal{L}_1$ and $\mathcal{L}_5$ is known ($\mathcal{L}_1/\mathcal{L}_5 = -\exp(2ikL)$ where $k = \omega/c$ is the wave number). Therefore the ratio I between the wave amplitude which the boundary condition should impose ($\mathcal{L}_5^t$) and the wave which will actually be imposed ($\mathcal{L}_5$) by Eq. (24) can also be expressed as:

$$I = \frac{\hat{\mathcal{L}}_5}{\hat{\mathcal{L}}_5^t} = \frac{1}{1 + R_1\exp(2ikL)} \tag{29}$$

I is a deterioration index: when it is equal to unity, the boundary condition is perfect, the injected wave is the one imposed by the user and the inlet velocity is $u = \bar{u} + u_a^t + u_-$ which is the exact solution. Any non unity I value indicates that the relaxation term in Eq. (24) is perturbing the inlet boundary condition and making it partially reflecting. Obviously for the NRI-NSCBC condition where $\alpha = 1$ and $R_1 = 0$, I is equal to unity for all K values while it is not for the standard NSCBC approach. To check this result, one-dimensional simulations of the configuration of Fig. 5 were performed for $\sigma = 0$, 2 and 5 at three forcing frequencies (100, 200

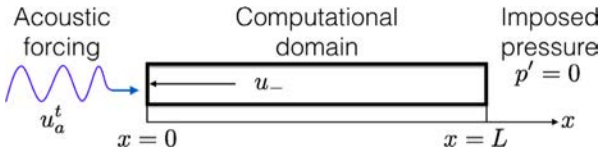

Fig. 5. Tests of inlet boundary conditions for a one-dimensional duct forced by a harmonic wave at the inlet and terminated by a pressure node at $x = L$.

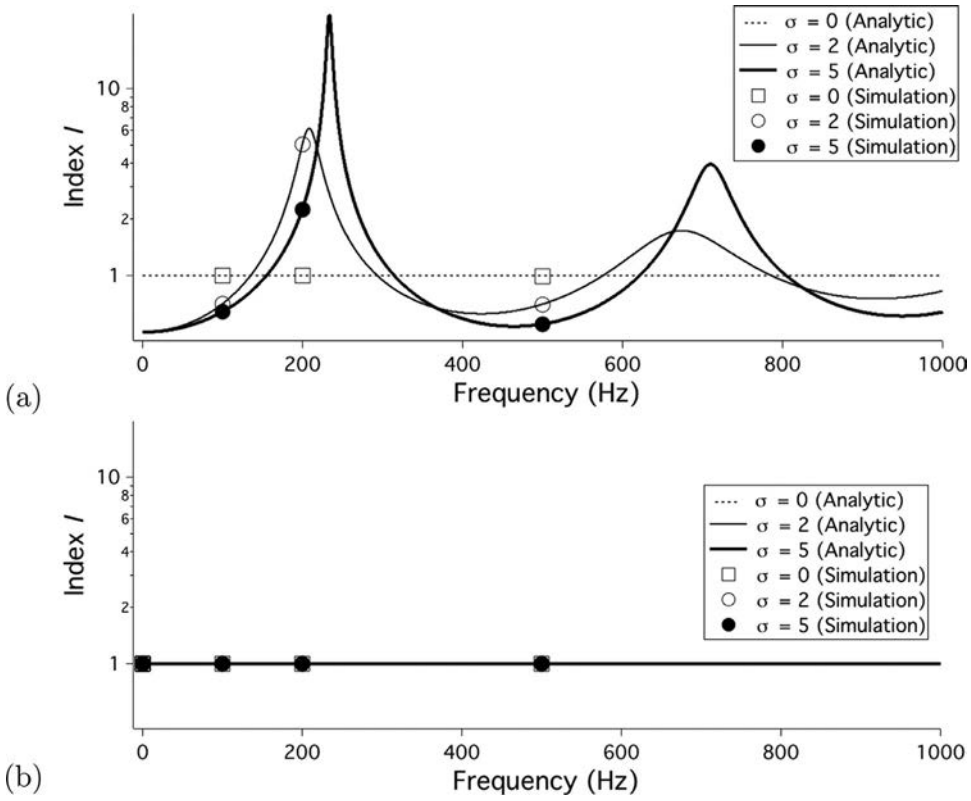

Fig. 6. Comparison of the quality index I (Eq. 29) in log scale, for the pulsated duct of Fig. 5: analytical result (Eq. (29)) vs compressible simulations. (a) standard NSCBC method, (b) new NRI-NSCBC method. Lines: analytical solutions; symbols: simulations.

and 500 Hz). The results obtained in terms of the index I as a function of the reduced relaxation coefficient σ are displayed in Fig. 6. The simulations match exactly the analytical result of Eq. (29) and confirm that for the NSCBC standard formulation, the deterioration index I can reach large values more than 20 for $\sigma = 5$), indicating that this method is much less accurate than the new NRI-NSCBC condition which offers a unity I index for all values of the relaxation coefficient σ. These results confirm the analysis of Polifke et al. [1] who pointed out the importance of taking u_- into account in the relaxation term.

6. Faster convergence for unforced compressible flows

The capabilities of the NRI-NSCBC can be illustrated in a second test, to demonstrate that it allows faster convergence in multi-dimensional, compressible, unforced flows because acoustic waves are perfectly evacuated through the boundaries while avoiding a drift of mean values, thanks to a large value of the inlet relaxation coefficient K. For an unforced flow ($u_a^t = u_v^t = 0$), the inlet wave of Eq. (22) becomes:

$$\mathcal{L}_5 = 2\ K\rho c[u - \bar{u}] \quad \text{for NSCBC} \tag{30}$$

and

$$\mathcal{L}_5 = 2\ K\rho c[u - (\bar{u} + u_-)] \quad \text{for NRI} - \text{NSCBC} \tag{31}$$

The test case is a two-dimensional subsonic nozzle (Fig. 7) where the inlet Mach number is 0.014, corresponding to an inlet velocity of 5 m/s. The outlet condition is $p' = 0$. The initial condition corresponds to a zero velocity field and constant pressure and temperature everywhere in the domain, including on the inlet patch. The shape of the nozzle is given by (unit m):

$$y = \begin{cases} 0.02\left[1.0 - 0.661514e^{\left(-\ln\ 2(x/0.6)^2\right)}\right], & x < 0 \\ 0.02\left[1.0 - 0.661514e^{\left(-\ln\ 2(x/6)^2\right)}\right], & x \geq 0 \end{cases} \tag{32}$$

When the simulation begins, the inlet boundary condition starts modifying the inlet variables. The objective of the test is to measure the physical time required for the simulation to reach steady state and to check whether acoustic modes of the configuration are triggered.

This flow is a good prototype of many compressible simulations. The initial conditions (zero velocity everywhere) combined with the inlet condition (which ramps rapidly to its target value) can generate strong perturbations and acoustic waves: with the standard NSCBC conditions (Fig. 3), low values of K lead to mean values which do not converge to the target values or drift away from them. On the other hand, large values of K avoid drifting mean

Fig. 7. Geometry of nozzle used for convergence tests to steady state. The domain length is $L = 0.6$m. The sound speed is $c = 345$ m/s.

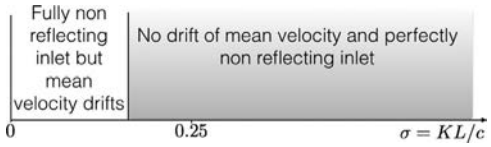

Fig. 8. Typical behavior of the solution for the new NRI-NSCBC inlet condition as a function of the reduced relaxation coefficient $\sigma = KL/c$. L is a typical domain length and c the sound speed. The shaded area is the desired operational zone.

values but induce reflections and undamped acoustic waves which delay convergence. With NRI-NSCBC, this problem disappears: it is possible to use large values of K and still be non reflecting so that convergence is reached very fast. Fig. 8 summarizes this observation and can be compared to Fig. 3.

Fig. 9 displays a typical time evolution of inlet velocity and pressure for a reduced relaxation coefficient $\sigma = KL/c = 0.017$. Since this coefficient is small, the inlet velocity (Fig. 9, left) increases slowly and no acoustic waves are triggered. However, convergence is reached after a long time for both methods (NSCBC in solid line and NRI-NSCBC in dashed line).

To increase the convergence speed, the natural solution is to increase the inlet relaxation factor: Fig. 10 shows the solutions for a reduced relaxation coefficient $\sigma = KL/c = 17$. The inlet velocity rapidly reaches its target (5 m/s) but acoustic oscillations are triggered using the classical NSCBC method (solid line) because acoustic waves are trapped within the domain: pressure and velocity oscillate at 150 Hz which is the frequency of the first mode of the setup with $u' = 0$ at the inlet and $p' = 0$ at the outlet. Inversely, the NRI-NSCBC method gives a solution (dashed line) which is stabilized after one acoustic time.

Increasing the relaxation coefficient even more (as often done by NSCBC users when they observe an oscillating inlet velocity) does stabilize the inlet velocity (Fig. 11, left) but makes the inlet even more reflecting, leading to pressure inlet excursions which actually grow in time (Fig. 11, right) and a boundary condition which is ill posed and will eventually lead to full divergence. NRI-NSCBC, as expected, is only weakly affected by the increase of σ and leads to a stable solution rapidly. This simple example reveals another interesting feature of the NRI-NSCBC condition, which provides fast convergence to steady state, using large relaxation coefficients, a useful property in all compressible solvers.

7. Simultaneous injection of turbulence and acoustic waves through a non-reflecting inlet

This test case corresponds to a situation where an inlet ($x = 0$ in Fig. 12) is used to inject both turbulence and an harmonic acoustic wave into a square section channel. The domain is a three-dimensional parallelepipedic box where the outlet is fully reflecting (imposed pressure: $p' = 0$ at $x = L$). Therefore, the inlet is submitted to three waves:

- vorticity waves associated to the turbulence injection u_v^t,
- an ingoing acoustic wave associated to the acoustic forcing u_a^t,
- an outgoing acoustic wave reflected from the outlet and propagating back to the inlet u_-.

The mesh is a pure hexahedra grid with $392 \times 98 \times 98$ points corresponding to a domain size of $L = 4 \times 1 \times 1$ mm. The mean inlet velocity is homogeneous in the $x = 0$ plane: $U = 100$ m/s. Periodicity conditions are applied in the two transverse directions y and z. Very large values of the relaxation coefficient K are used in both NSCBC and NRI-NSCBC: $K = 2.10^6 s^{-1}$ corresponding to a reduced coefficient $\sigma = KL/c = 23$. The inlet is submitted to two simultaneous outside excitations:

1. Three-dimensional turbulence: the RMS velocity of the injected turbulent field is $u^t_{v,RMS} = 5$ m/s and its most energetic wavelength is 0.5 mm. The turbulence spectrum has a Passot Pouquet expression [45].
2. One-dimensional planar acoustic wave: the acoustic forcing is a longitudinal harmonic wave introduced at the domain inlet, at a frequenc $f = 260$ kHz with a peak amplitude of $u^t_{a,peak} = 2$ m/s.

Note that the ratio between the two excitations levels can be fixed arbitrarily and is configuration dependent. It is measured here by the ratio of the excitation velocities $u^t_{v,RMS}/u^t_{a,peak} = 2.5$.

Fig. 13 displays fields of Q-criterion [46] for the standard NSCBC (left) and the NRI-NSCBC approaches (right), showing a usual decaying turbulent field. The same figure displays a pressure field in one plane, revealing that the axial plane acoustic forcing can be identified on the pressure signal. These qualitative results require more analysis to see the influence of the boundary condition. Fig. 14 shows the FFTs of pressure (left) and velocity (right) at the inlet ($x = 0$ m).

The two velocity spectra (right image) of Fig. 14 are close and both boundary conditions (NSCBC and NRI-NSCBC) produce inlet fluctuations which match the spectra of the target velocity u_t very well, confirming that the turbulent signal is correctly introduced. Note that no discrete peak is visible at the acoustic forcing frequency ($f = 260$ kHz). For the conditions chosen here ($u^t_{a,peak}/u^t_{v,RMS} = 0.4$), the acoustic forcing is not strong enough to dominate the turbulent forcing. For pressure (left image), however, the two spectra differ: both exhibit a peak at the acoustic forcing frequency (and its first harmonic) but the NSCBC results also

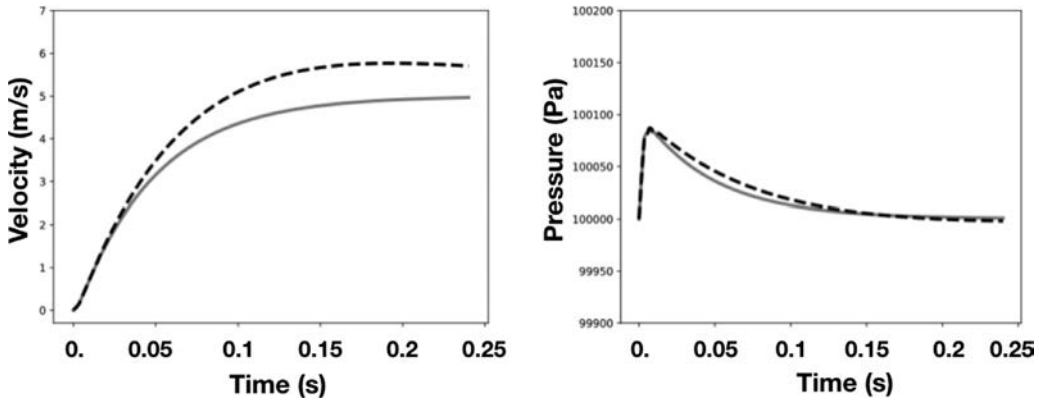

Fig. 9. Inlet velocity (left) and pressure (right) time evolutions for $\sigma = KL/c = 0.017$. NSCBC: solid line. NRI-NSCBC: dashed line.

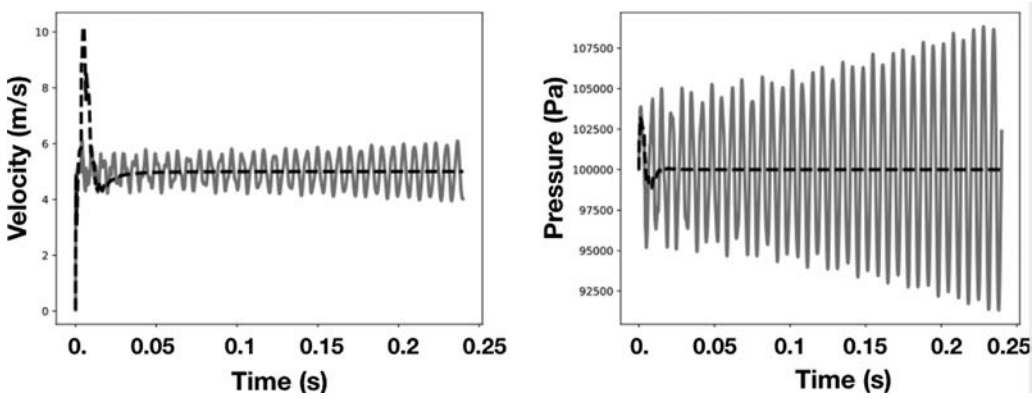

Fig. 10. Inlet velocity (left) and pressure (right) time evolutions for $\sigma = KL/c = 17$. NSCBC: solid line. NRI-NSCBC: dashed line.

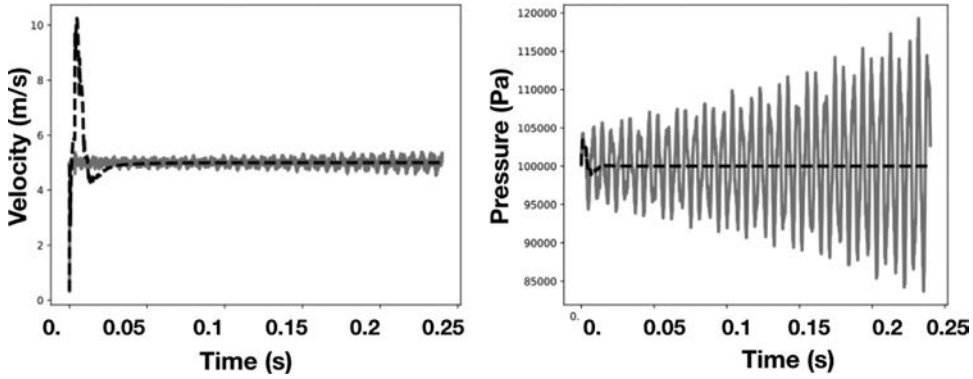

Fig. 11. Inlet velocity (left) and pressure (right) time evolutions for $\sigma = KL/c = 170$. NSCBC: solid line. NRI-NSCBC: dashed line.

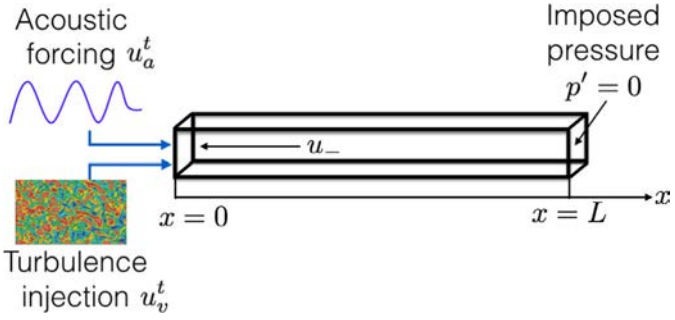

Fig. 12. Simultaneous injection of three-dimensional turbulence (velocity amplitude u_v^t) and one-dimensional acoustic forcing (velocity amplitude u_a^t) at the inlet of a domain with reflecting outlet ($p' = 0$).

reveal multiple other peaks due to non physical resonances. It is interesting to compare the pressure field obtained in the LES with the analytical solution corresponding to a forced inlet at frequency f and an outlet condition $p' = 0$. In a laminar flow (in the absence of turbulence injection), taking into account the correction due to non-zero Mach number, this solution is:

$$p'(x,t) = \rho c u_a \left(e^{-ik^+x} - e^{-i(k^+L+k^-(L-x))}\right)e^{i\omega t} \tag{33}$$

and

$$u'(x,t) = u_a \left(e^{-ik^+x} + e^{-i(k^+L+k^-(L-x))}\right)e^{i\omega t} \tag{34}$$

where $k^+ = \omega/(c+u)$, $k^- = \omega/(c-u)$ and $\omega = 2\pi f$. The variance of pressure p'^2 can be obtained by $p'^2 = p_a p_a^*/2$, with p_a^* the conjugate complex of p_a. Fig. 15 shows variations of $\sqrt{p'^2}$ along the duct axis for both boundary conditions and compares it to the analytical solution of Eq. (33). The NRI-NSCBC captures perfectly the analytical solution showing that for these conditions ($u_t/u_a = 2.5$), the unsteady pressure field is only weakly affected by the turbulence injection and that the NRI-NSCBC condition does not alter this property. On the other hand, similarly to the case of acoustic forcing in a laminar flow (Section 5), the classical NSCBC formulation modifies the acoustic field structure and fails to capture the analytic solution.

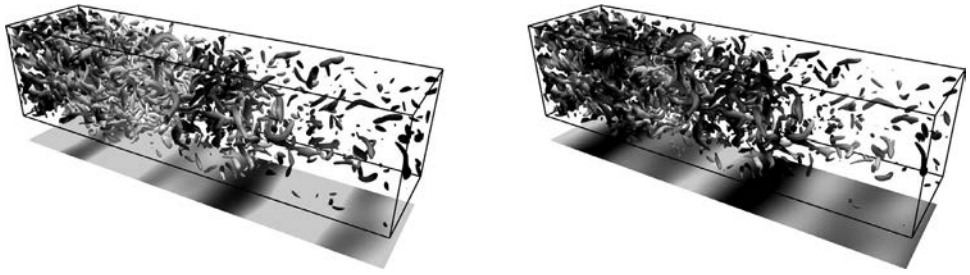

Fig. 13. Simultaneous injection of isotropic homogeneous turbulence and acoustic wave. Isosurface of Q criterion $Q = 2.5(U/L)^2$ colored by the axial velocity ($95 \leq u(m/s) \leq 105$) and fluctuating pressure in the range $-1.2e-2 \leq p/p_\infty - 1 \leq 1.2e-2$ in one plane. Left: NSCBC, right: NRI-NSCBC.

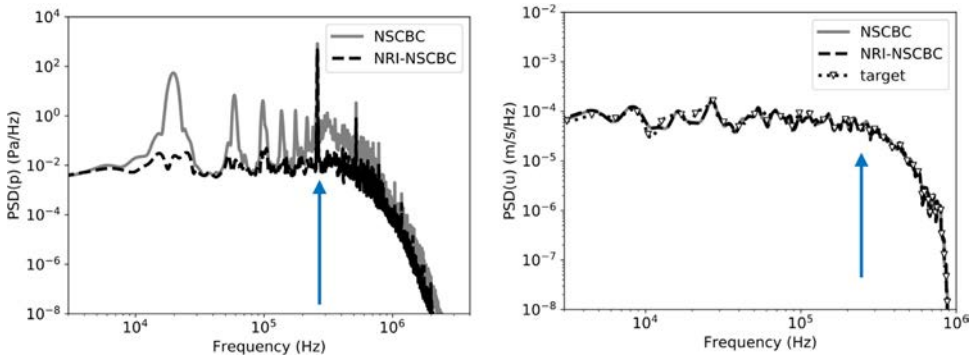

Fig. 14. Simultaneous injection of isotropic homogeneous turbulence and acoustic wave. Spectra of pressure (left) and velocity (right) at the domain inlet $x = 0$ m, $y = z = 0.005$ m. Solid line: NSCBC, dashed line: NRI-NSCBC. The arrows indicate the frequency ($f_a = 260$ kHz) at which the acoustic wave is introduced. The triangles on the right image correspond to the spectra of the injected turbulence target signal u_v^t.

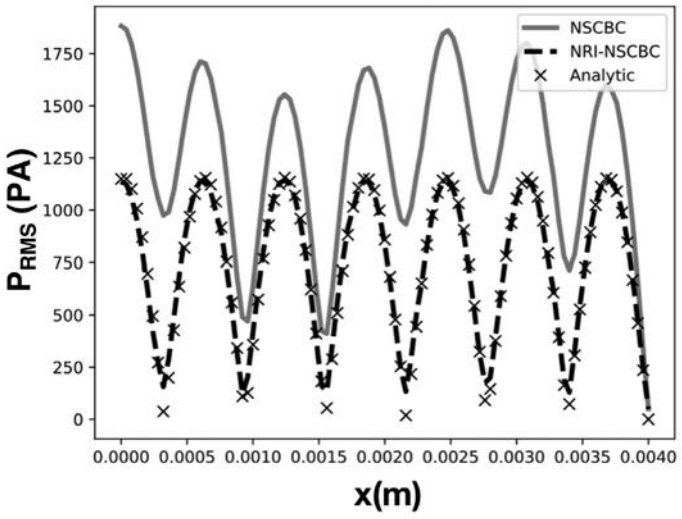

Fig. 15. Pressure perturbation structure along duct axis: field of $\sqrt{(p'^2)}$ vs x. Solid line: NSCBC, dashed line: NRI-NSCBC, symbols: analytical solution.

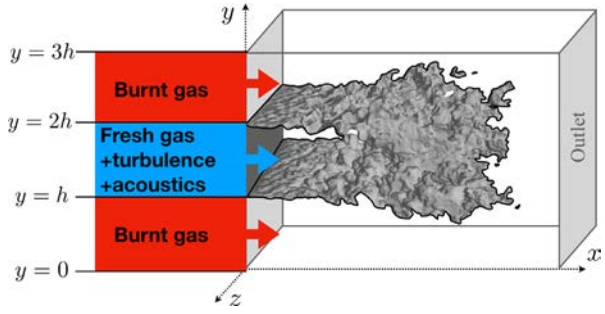

Fig. 16. Physical domain used for the DNS. At the inlet, a double hyperbolic tangent profile is used to inject fresh gases in a sheet ≈8 mm high, surrounded by a coflow of burnt gases. Top-bottom (along y) and left-right (along z) boundaries are periodic. The isosurface is a typical view of $T = 1600$ K.

8. A turbulent, acoustically forced premixed flame

The last example is a direct numerical simulation (DNS) of a stoichiometric, premixed turbulent flame stabilized in a slot-burner configuration. The inlet is forced by turbulence and by an harmonic acoustic wave introduced simultaneously, a usual situation for example to study Flame Transfer Functions in thermoacoustics.

The DNS is performed with the explicit, compressible solver (AVBP) for the 3D Navier–Stokes equations with simplified thermochemistry on unstructured meshes [43,47]. A Taylor–Galerkin finite element scheme called TTGC [42] of fourth-order in space and time is used. The acoustic CFL number is 0.7. The outlet boundary condition is handled using an imposed pressure, NSCBC approach [3] with transverse terms corrections [37]. The inlet is treated either with the standard NSCBC formulation or with the new NRI-NSCBC approach. Other boundaries are treated as periodic.

Methane/air chemistry at 1 bar is modeled using a global 2-step scheme fitted to reproduce the flame propagation properties such as the flame speed, the burned gas temperature and the flame thickness [48]. This simplified chemistry description is sufficient to study the dynamics of premixed turbulent flames. Fresh gases are stoichiometric: the laminar flame speed is $S_L^0 = 40.5$ cm/s. The flame thicknesses are $\delta_L^0 = 0.34$ mm (based on the maximum temperature gradient) and $\delta_L^1 = 0.7$ mm (based on the distance between reduced temperatures of 0.01 and 0.99). The mesh is a homogeneous hexahedra grid with a constant element size $\Delta x = 0.1$ mm, ensuring 7–9 points in the preheat zone and 4–5 in the reaction zone. With this resolution, the temperature and heat release profiles given by the DNS code match perfectly the results given by a specialized one-dimensional flame code (Cantera) for a laminar premixed flame. The domain size is 512 cells (5,12 cm) in the x direction and 256 cells (2,56 cm) in the y and z ones, for a total of 33.55 million cells (Fig. 16). The fresh gas injection channel has a height $h = 8.53$ mm ($h/\delta_L^0 \approx 25$).

The inlet stream is a central flow of stoichiometric fresh gases surrounded by a coflow of burnt gases at low injection velocity. Inlet temperatures are 300 and 2256 K in the fresh and burnt gases, respectively. The temperature and composition of the burnt gas coflow corresponds to the products of an adiabatic combustion of the fresh gases. Mean inlet velocity profiles are imposed as:

$$u(x=0,y,z) = u_{co} + (u_{in} - u_{co})\left(1 + \tanh\left(\frac{y-h}{2\delta}\right)\right) \times \left(1 - \tanh\left(\frac{y-2h}{2\delta}\right)\right) \quad (35)$$

where $u_{in} = 10$ m/s is the maximum speed in the fresh gases, $u_{co} = 0.1$ m/s is the minimum speed in the coflow of hot gases and δ is the momentum thickness of the shear layer ($\delta = 0.08$ mm) corresponding to a vorticity thickness of 0.36 mm. Turbulence is injected in the fresh gases only. The RMS velocity of the incoming flow is 1 m/s and the integral length scale is $l_F = 2$ mm. The spectrum of the injected turbulence corresponds to a Passot–Pouquet form [45]. Acoustic forcing is introduced at the inlet on the fresh gas stream. The forcing frequency is $f_a = 1$ kHz and the forcing amplitude is 2 m/s. For both NRI-NSCBC and NSCBC

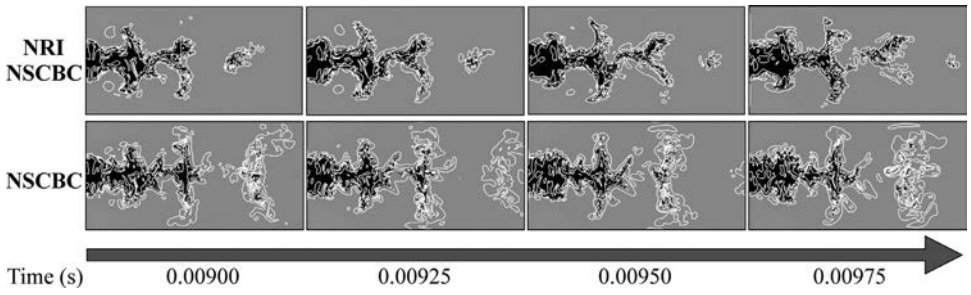

Fig. 17. Flame response at four instants of the acoustic forcing period ($f_a = 1$ kHz). Temperature field and isolevels of vorticity.

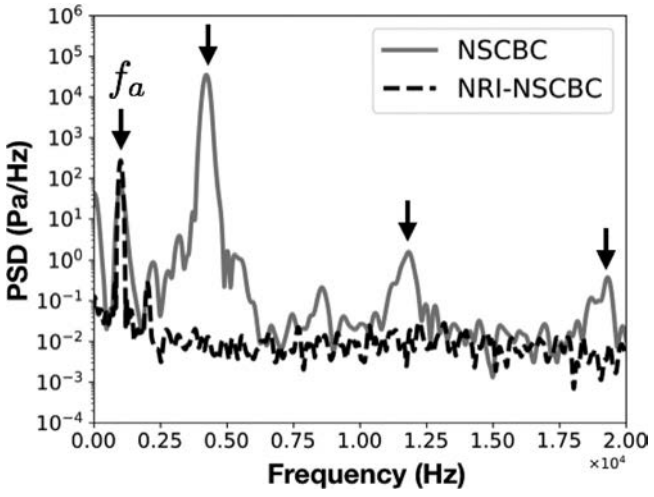

Fig. 18. Pressure spectra for NSCBC (solid line) and NRI-NSCBC (dotted line) at the domain inlet. The f_a arrow corresponds to the acoustic forcing at 1 kHz. The three other arrows are the first three longitudinal eigenmodes of the computational box at 4350, 12500 and 19500 Hz. The spectral resolution is 70 Hz.

conditions imposed at the inlet, the value of K is the same: $K = 100000$ s^{-1} (leading to $\sigma \simeq 15$). A series of 4 snapshots showing the flame response to turbulent and acoustic forcing is displayed in Fig. 17. Mushroom-shaped flame structures are created at 1 Khz as expected for acoustically forced flames [49]. These structures are separated spatially by $u_{in}/f_a = 1$ cm and interact with the injected turbulence.

The two DNS of Fig. 17, obtained by NRI-NSCBC and NSCBC, are obviously different but it is difficult to say which one is the best. A more quantitative result can be obtained by looking at the pressure spectra at the domain inlet in Fig. 18. The spectra observed for NRI-NSCBC corresponds to the expected result: a discrete peak at the acoustic forcing frequency f_a superimposed on broadband turbulent noise. On the other hand, for NSCBC, three additional high-level peaks also appear: they are due to the excitation by the flame of the eigenmodes of the computational domain. It is possible to verify that these modes are indeed acoustic modes by using an Helmholtz solver [50] taking into account the mean temperature distribution in the domain and the boundary conditions (imposed inlet velocity and imposed outlet pressure). The frequencies predicted for the first three acoustic modes given by the Helmholtz solver are marked by arrows in Fig. 18. The three acoustic modes which are excited when NSCBC is used are the longitudinal 1/4 wave (at 4350 Hz), 3/4 wave (at 12500 Hz) and 5/4 wave (at 19500 Hz) modes. Their frequencies, computed with the Helmholtz solver, match the frequencies observed in the LES with a 5 percent accuracy. These modes interact with the flame response at the acoustic forcing frequency ($f_a = 1$ kHz) and make the NSCBC run difficult to interpret: measuring the flame response at $f_a = 1$ kHz would be impossible for the NSCBC run because this response is polluted by the three acoustic eigenmodes forced by the boundary conditions. Clearly, NSCBC fails to inject acoustic forcing and turbulence without exciting the cavity modes of the computational domain while NRI-NSCBC succeeds in this task.

9. Conclusions

This paper has described a new boundary condition for subsonic inlet, based on a combination of the formalism proposed by Polifke and coworkers [1,2] to account for outgoing acoustic waves and an extension of the method of Guezennec et al.[40] to introduce both turbulence and acoustic waves simultaneously. The approach can be summarized in the expression of the ingoing wave:

$$\frac{\mathcal{L}_5}{\rho c} = -2\frac{\partial u_a^t}{\partial t} - \frac{\partial u_v^t}{\partial t} + 2\ K[u - (\bar{u} + u_a^t + u_v^t + u_-)] \tag{36}$$

where u_a^t is the velocity of the injected acoustic wave, u_v^t is the axial velocity of the turbulent signal, $\bar{u}$ is the mean target velocity, K is a relaxation coefficient and u_- is the velocity of the outgoing wave which is estimated locally using the outgoing wave amplitude $\mathcal{L}_1$:

$$u_- = \frac{1}{2\rho c}\int_0^t \mathcal{L}_1 dt \tag{37}$$

Analysis and tests show that this NRI-NSCBC condition performs better than the standard NSCBC approach: it allows to use large values for the relaxation coefficient K and to obtain non-drifting mean values and non reflective capabilities simultaneouslyecor. Tests were performed for one-dimensional acoustic forcing in a duct, for flow establishment in a compressible nozzle, for simultaneous injection of acoustic waves and turbulence in a three-dimensional channel terminated by a fixed pressure outlet and finally for a turbulent premixed flame forced acoustically. For all cases, NRI-NSCBC captured the expected solution accurately suggesting that this could become a standard approach in compressible codes.

Acknowledgments

We thank Dr L. Selle (IMF Toulouse, CNRS) for helpful discussions and the CERFACS CFD team staff for their scientific and technical support about the CFD code AVBP. The contribution of V. Bouillin to the development of NRI-NSCBC is gratefully acknowledged.

References

[1] Polifke W, Wall C, Moin P. Partially reflecting and non-reflecting boundary conditions for simulation of compressible viscous flow. J Comput Phys 2006;213(1):437–49.
[2] Tudisco P, Ranjan R, Menon S, Jaensch S, Polifke W. Application of the time-domain impedance boundary condition to large-eddy simulation of combustion instability in a shear-coaxial high pressure combustor. Flow Turbul Combust 2017;177:1–23.

[3] Poinsot T, Lele S. Boundary conditions for direct simulations of compressible viscous flows. J Comput Phys 1992;101(1):104–29. doi:10.1016/0021-9991(92)90046-2.
[4] Thompson KW. Time dependent boundary conditions for hyperbolic systems ii. J Comput Phys 1990;89:439–61.
[5] Grappin R, Léorat J, Buttighoffer A. Alfvén wave propagation in the high solar corona. Astron Astrophys 2000;362:342–58.
[6] Freund JB. Proposed inflow/outlow boundary condition for direct computation of aerodynamic sound. AIAA 1997;35:740–2.
[7] Colonius T. Numerically nonreflecting boundary and interface conditions for compressible flow and aeroacoustic computations. AIAA 1997;35(7):1126–33.
[8] Colonius T, Lele SK. Computational aeroacoustics: progress on nonlinear problems of sound generation. Prog Aerosp Sci 2004;40(6):345–416.
[9] Bogey C, Bailly C. Effects of inflow conditions and forcing on subsonic jet flows and noise. AIAA 2005;43(5):1000–7.
[10] Pirozzoli S, Colonius T. Generalized characteristic relaxation boundary conditions for unsteady compressible flow simulations. J Comput Phys 2013;248(C):109–26.
[11] Lodato G, Domingo P, L V. Three-dimensional boundary conditions for direct and large-eddy simulation of compressible viscous flow. J Comput Phys 2008;227(10):5105–43.
[12] Poinsot T, Veynante D. Theoretical and numerical combustion. 3rd ed; 2011. (www.cerfacs.fr/elearning)
[13] Albin E, D'Angelo Y, Vervisch L. Using staggered grids with characteristic boundary conditions when solving compressible reactive Navier–Stokes equations. Int J Numer Methods Fluids 2011;68(5):546–63.
[14] Coussement A, Gicquel O, Caudal J, Fiorina B, Degrez G. Three-dimensional boundary conditions for numerical simulations of reactive compressible flows with complex thermochemistry. J Comput Phys 2012;231(17):5571–611.
[15] Poinsot T. Prediction and control of combustion instabilities in real engines (invited hottel lecture). Proc Combust Inst 2017:1–28.
[16] Lourier JM, Stöhr M, Noll B, Werner S, Fiolitakis A. Scale adaptive simulation of a thermoacoustic instability in a partially premixed lean swirl combustor. Combust Flame 2017;183:1–15.
[17] Krediet HJ, Beck CH, Krebs W, Schimek S, Paschereit CO, Kok JBW. Identification of the flame describing function of a premixed swirl flame from les. Combust Sci Technol 2012;184(7–8):888–900.
[18] Duran I, Moreau S, Poinsot T. Analytical and numerical study of combustion noise through a subsonic nozzle. AIAA 2013;51(1):42–52.
[19] Dowling AP, Mahmoudi Y. Combustion noise. Proc Combust Inst 2015;35(1):65–100.
[20] Ihme M. Combustion and engine-Core noise. Ann Rev Fluid Mech 2016;49:1–35.
[21] Ni F, Miguel-Brebion M, Nicoud F, Poinsot T. Accounting for acoustic damping in a helmholtz solver. AIAA 2017;55(4):1205–20.
[22] Abom M. A note on the experimental determination of acoustical two-port matrices. J Sound Vib 1991;155(1):185–8.
[23] Polifke W, Poncet A, Paschereit CO, Doebbeling K. Reconstruction of acoustic transfer matrices by instationnary computational fluid dynamics. J Sound Vib 2001;245(3):483–510.
[24] Tournadre J, Förner K, Polifke W, Martínez-Lera P, Desmet W. Determination of acoustic impedance for Helmholtz resonators through incompressible unsteady flow simulations. AIAA 2016:1–9.
[25] Magri L, O'Brien J, Ihme M. Compositional inhomogeneities as a source of indirect combustion noise. J Fluid Mech 2016;799:R4–1.
[26] Livebardon T, Moreau S, Gicquel L, Poinsot T, Bouty E. Combining LES of combustion chamber and an actuator disk theory to predict combustion noise in a helicopter engine. Combust Flame 2016;165:272–87.
[27] Thompson KW. Time dependent boundary conditions for hyperbolic systems. J Comput Phys 1987;68:1–24.
[28] Giles M. Non-reflecting boundary conditions for euler equation calculations. AIAA 1990;28(12):2050–8.
[29] Yoo C, Wang Y, Trouvé A, Im H. Characteristic boundary conditions for direct simulations of turbulent counterflow flames. Combust Theor Model 2005;9:617–46.
[30] Yoo C, Im H. Characteristic boundary conditions for simulations of compressible reacting flows with multi-dimensional, viscous, and reaction effects. Combust Theor Model 2007;11:259–86.
[31] Berenger J-P. A perfectly matched layer for the absorption of electromagnetic waves. J Comput Phys 1994;114(2):185–200.
[32] Tam C. Advances in numerical boundary conditions for computational aeroacoustics. J Comput Phys 1998;6(4):377–402.
[33] Hu FQ, Li X, Lin D. Absorbing boundary conditions for nonlinear euler and Navier–Stokes equations based on the perfectly matched layer technique. J Comput Phys 2008;227(9):4398–424.
[34] Selle L, Nicoud F, Poinsot T. The actual impedance of non-reflecting boundary conditions: implications for the computation of resonators. AIAA 2004;42(5):958–64.
[35] Tudisco P, Ranjan R, Menon S, Jaensch S, Polifke W. Simulation of transverse combustion instability in a multi-injector combustor using the time -domain impedance boundary conditions. Flow Turbul Combust 2018;101:55–76.
[36] Rudy DH, Strikwerda JC. A non-reflecting outflow boundary condition for subsonic Navier Stokes calculations. J Comput Phys 1980;36:55–70.
[37] Granet V, Vermorel O, Leonard T, Gicquel L, Poinsot T. Comparison of nonreflecting outlet boundary conditions for compressible solvers on unstructured grids. AIAA 2010;48(10):2348–64.
[38] Rudy DH, Strikwerda JC. Boundary conditions for subsonic compressible Navier Stokes calculations. Comput Fluids 1981;9:327–38.
[39] Prosser R. Improved boundary conditions for the direct numerical simulation of turbulent subsonic flows i: inviscid flows. J Comput Phys 2005;207:736–68.
[40] Guezennec N, Poinsot T. Acoustically nonreflecting and reflecting boundary conditions for vorticity injection in compressible solvers. AIAA 2009;47:1709–22.
[41] Kopitz J, Brocker E, Polifke W. Characteristics-based filter for identification of acoustic waves in numerical simulation of turbulent compressible flow.. 12th Int'l Congress on Sound and Vibration (ICSV 12); 2005. Lisbon, Portugal
[42] Colin O, Rudgyard M. Development of high-order Taylor–Galerkin schemes for unsteady calculations. J Comput Phys 2000;162(2):338–71.
[43] Schønfeld T, Rudgyard M. Steady and unsteady flows simulations using the hybrid flow solver avbp. AIAA 1999;37(11):1378–85.
[44] Gourdain N, Gicquel L, Montagnac M, Vermorel O, Gazaix M, Staffelbach G, et al. High performance parallel computing of flows in complex geometries: I. Methods. Comput Sci Disc 2009;2(1):015003.
[45] Passot T, Pouquet A. Numerical simulation of compressible homogeneous flows in the turbulent regime. J Fluid Mech 1987;181:441–66.
[46] Hussain F, Jeong J. On the identification of a vortex. J Fluid Mech 1995;285:69–94.
[47] Selle L, Lartigue G, Poinsot T, Koch R, Schildmacher K-U, Krebs W, et al. Compressible large-eddy simulation of turbulent combustion in complex geometry on unstructured meshes. Combust Flame 2004;137(4):489–505.
[48] Franzelli B, Riber E, Gicquel LY, Poinsot T. Large eddy simulation of combustion instabilities in a lean partially premixed swirled flame. Combust Flame 2012;159(2):621–37.
[49] Poinsot T, Trouvé A, Veynante D, Candel S, Esposito E. Vortex driven acoustically coupled combustion instabilities. J Fluid Mech 1987;177:265–92.
[50] Nicoud F, Benoit L, Sensiau C, Poinsot T. Acoustic modes in combustors with complex impedances and multidimensional active flames. AIAA 2007;45:426–41.